Title:

Large Eddy Simulation of an Ethanol Spray Flame Under MILD Combustion with the Stochastic Fields Method

Authors:

S. Gallot-Lavallée, Department of Mechanical Engineering, Imperial College London

W. P. Jones, Department of Mechanical Engineering, Imperial College London

A. J. Marquis, Department of Mechanical Engineering, Imperial College London

Corresponding Author:

Simon Gallot Lavallée

Department of Mechanical Engineering,

Imperial College London,

South Kensington Campus

Exhibition Road

SW7 2AZ, London, UK

email: simon.gallot-lavallee@imperial.ac.uk

Colloquium:

Spray, Droplet And Supercritical Combustion.

Length Of the Paper:

Method 2 Adopted.

Total length of paper: 5785 words.

Word equivalent length for main text: 3552 words.

Word equivalent length for figures: Figure 1 250 words, Figure 2 170 words, Figure 3 180 words, Figure 4 180 words, Figure 5 180 words, Figure 6 180 words, Figure 7 190 words, Figure 8 190 words, Figure 9 180 words

Word equivalent length for tables: Table 1 60 words.

Word equivalent length for references: 473 words.

List of Tables

List of Figures

Large Eddy Simulation of an Ethanol Spray Flame Under MILD Combustion with the Stochastic Fields Method

S. Gallot-Lavallée*, W. P. Jones, A. J. Marquis

Department of Mechanical Engineering
Imperial College London
Exhibition Road, London, SW7 2AZ, UK

Abstract

A combustion device operating in Moderate or Intense Low-oxygen Dilution (MILD) condition is numerically simulated. The burner consists of a cylindrical hot co-flow generator with an injector installed on the central axis. The hot co-flow is obtained by the lean combustion of Dutch Natural Gas (DNG). The spray is injected through an industrial pressure swirl atomiser using liquid ethanol as fuel. MILD combustion consists in burning the fuel in a high temperature environment so that the temperature gradients are limited and the production of pollutants such as NO_x reduced. MILD combustion has been investigated for furnace applications and for various gaseous fuels, recently it has also been explored for spray combustion. The simulation is performed in the context of Large Eddy Simulation (LES) and the transported pdf equation for the scalars is solved using the stochastic fields approach. The validation of the results is based on the comparison with experimental data. The characteristics of the injector are obtained *a posteriori* by the use of the measurements at downstream location. The simulation correctly reproduces the velocity profiles of the particles within their size classes and the integral particle size distribution which is represented by the Sauter Mean Diameter (SMD). The gas phase temperature and velocity are also in good agreement with the measurements, however, some discrepancies are observed, presumably because of the lack of modelling of primary atomisation. The model employed appears to reliably reproduce the behaviour of the spray combustion system under MILD conditions.

Keywords: Large Eddy Simulation, Stochastic Fields Method, MILD Combustion, Ethanol, Spray Combustion

*Corresponding author
Email address: simon.gallot-lavallee@imperial.ac.uk (S. Gallot-Lavallée)

1. Introduction

Research in combustion science is driven by two major challenges: the need for cleaner combustion systems and the improvement of combustion efficiency. Among the pollutants generated NO_x has been identified as highly hazardous for human health and therefore its emissions need to be minimised. NO_x is generated when high temperature and high oxygen concentrations are present in the flame. To reduce the flame temperature various techniques are available such as Exhaust Gas Recirculation (EGR) which is well established and widely used. However EGR has important restrictions on the recirculation rates (related to oxygen concentration) that must be limited in order to maintain a stable flame. It was found that in particular conditions it is possible to attain high rates of recirculation with small temperature gradients in the flame but high ambient temperatures. This allows for low NO_x production and a good efficiency. This technique is named Moderate or Intense Low-oxygen Dilution (MILD) [1] or "flameless" combustion [2]. It was originally developed in Japan where is known as High Temperature Air Combustion (HTAC) [3]. The accurate definition of MILD combustion by Cavaliere et al. [1] states that the temperature of the reactants must be higher than the auto-ignition temperature of the fuel, and that the temperature change in the system should be lower than the auto-ignition temperature of the fuel. It is important in the design of industrial burners to have models able to predict such combustion regimes accurately at limited computational cost. DNS studies provided a fundamental insight of MILD combustion regime, however they are unsatisfactory in terms of applicability at industrial scales [4, 5]. The prediction of NO_x production has been simulated using RANS together with the unsteady flamelet model by Celho et al. [6] providing good results in terms of the velocity field with the NO levels obtained being of the same order of magnitude as those measured. However, following a need to provide more accurate and reliable computational methods the present work focuses on LES. The demand of flexibility in fuel utilisation has increased the interest in liquid fuels and for this reason a spray fuelled, experimentally studied MILD combustor configuration has been selected as a target for model validation. The measurements were conducted at TU Delft and further details can be found in the works by Roekaerts et al. [8, 9]. The same group also completed a numerical study investigating the same set-up using RANS starting their simulations at the first measurement location with good results [11]. The present work focuses on the applicability of the LES-pdf approach to MILD combustion together with the stochastic fields method for the continuous phase and a stochastic Lagrangian particles description of the dispersed phase. The method has already been applied to a gas turbine combustor [12], methanol spray flame [13] and to the Sandia n-heptane spray flame [14] amongst others. The pdf method is used to model the interaction between turbulence and chemistry in a Eulerian framework. In particular the stochastic field

method is applied for the solution of the evolution of the joint sub-grid scale pdf. The particles are simulated using the Lagrangian point source approach due to the dilute regime condition; the particle interactions with the sub grid scale fluctuations are represented using a stochastic approach.

2. Mathematical Modelling

2.1. Continuous Phase

The filtered forms of mass and momentum equation for low Mach number flows are as follow:

$$\frac{\partial \overline{\rho}_g}{\partial t} + \frac{\partial (\overline{\rho}_g \widetilde{u}_j)}{\partial x_j} = \bar{\dot{m}} \tag{1}$$

$$\begin{aligned} \frac{\partial (\overline{\rho}_g \widetilde{u}_j)}{\partial t} + \frac{\partial (\overline{\rho}_g \widetilde{u}_i \widetilde{u}_j)}{\partial x_j} = & -\frac{\partial \bar{p}}{\partial x_i} + \frac{\partial}{\partial x_j}\left(2\mu \bar{e}_{ij}\right) + \\ & - \frac{\partial \tau_{ij}^{sgs}}{\partial x_j} + \bar{\rho} g_i + \bar{\dot{m}}_m \end{aligned} \tag{2}$$

where ρ_g, μ, u, and p represent the fluid density, viscosity, velocity and static pressure respectively. The tensors e_{ij} and τ_{ij}^{sgs} are the strain rate and sub-grid scale (sgs) stress tensor. The latter, defined as $\tau_{ij}^{sgs} = \overline{\rho}_g \left(\widetilde{u_i u_j} - \tilde{u}_i \tilde{u}_j\right)$, is computed using the dynamically calibrated version of the Smagorinsky model by Piomelli and Liu [15]. The filtered forms of the conservation equations for the specific molar mass of the chemical species contain the filtered net formation rates of the chemical species through chemical reaction. The direct evaluation of these poses serious difficulties and to overcome these a joint sgs-pdf evolution equation formulation is adopted to determine species composition and energy. The modelled pdf equation is solved using the LES stochastic fields method, [17]. The combustion of ethanol-air is described using the 28 species reduced mechanism of Bhagatwala et al. [18]. The filtered forms of the conservation equations for species and enthalpy (ϕ_α with $1 \leq \alpha \leq N$ where N is equal to the number of species considered plus one) can be expressed as:

$$\begin{aligned} \frac{\partial \overline{\rho}_g \widetilde{\phi}_\alpha}{\partial t} + \frac{\partial \overline{\rho}_g \widetilde{\phi}_\alpha \widetilde{u}_j}{\partial x_j} = & \frac{\partial}{\partial x_j}\left(\frac{\mu}{\sigma}\frac{\partial \widetilde{\phi}_\alpha}{\partial x_j}\right) + \frac{\partial \mathscr{J}_j^{sgs}}{\partial x_j} + \\ & + \overline{\dot{m}}_\alpha \left(\underline{\phi}\right) + \overline{\rho_g \dot{\omega}_\alpha}\left(\underline{\phi}\right) \end{aligned} \tag{3}$$

where $\overline{\rho_g \dot{\omega}_\alpha}\left(\underline{\phi}\right)$ are the formation rates (sources) of species and enthalpy and $\mathscr{J}_j^{sgs}$ is the sub-grid scalar flux. The Lewis number is assumed to be unity so that σ represents the Schmidt or Prandtl number, as appropriate. The solution of the scalar fields is achieved using the joint sub-grid scale pdf evolution equation in conjunction with the Eulerian stochastic fields method [16]. The pdf is obtained from the solution of an

equivalent system of stochastic differential equations, where the n^{th} stochastic field ξ_α^n evolves according to:

$$\begin{aligned}\bar{\rho}\mathrm{d}\xi_\alpha^n = &-\bar{\rho}\tilde{u}_i\frac{\partial\xi_\alpha^n}{\partial x_i}\mathrm{d}t + \frac{\partial}{\partial x_i}\left[\Gamma'\frac{\partial\xi_\alpha^n}{\partial x_i}\right]\mathrm{d}t+\\ &+\bar{\rho}\sqrt{\frac{2\Gamma'}{\bar{\rho}}}\frac{\partial\xi_\alpha^n}{\partial x_j}\mathrm{d}W_i^n - \frac{\bar{\rho}}{2\tau_{sgs}}\left(\xi_\alpha^n - \widetilde{\phi}_\alpha\right)\mathrm{d}t+\\ &+\bar{\rho}\dot{\omega}_\alpha^n(\underline{\xi}^n)\mathrm{d}t + \left(\dot{m}_\alpha(\widetilde{\phi}_\alpha) - \dot{m}(\widetilde{\phi}_\alpha)\xi_\alpha^n\right)\mathrm{d}t\end{aligned} \tag{4}$$

where $1 < n < N_s$ with N_s being the number of stochastic fields. In the present case, eight stochastic fields were used, [20, 21, 14] The coupling between the gaseous and liquid phases is incorporated by the addition of terms representing the source of mass, momentum, and scalar quantities, $\bar{\dot{m}}$, $\bar{\dot{m}}_m$, and $\bar{\dot{m}}_\alpha$ through evaporation. Further details can be found in [14].

2.2. Dispersed Phase

Fuel droplets are described using the stochastic Lagrangian particle method described in [20, 21]. Droplet breakup is not included in the present work so droplets are described in terms of particle velocity, mass and temperature. Droplet size is very small compared to the LES filter width and they are therefore influenced both by the resolved gas phase properties and by the sub-grid scale fluctuations which are modelled as a Markov process, ie:

$$\begin{aligned}d\mathbf{V}^{(i)} = &\underbrace{\tau_p^{-1}\left(\widetilde{\mathbf{U}} - \mathbf{V}^{(i)}\right)\,dt + \left(1 - \frac{\rho_g}{\rho_\ell}\right)\mathbf{g}dt}_{deterministic}+\\ &\underbrace{+\left(C_0\frac{k_{sgs}}{\tau_t}\right)^{1/2}d\mathbf{W}_t}_{stochastic}\end{aligned} \tag{5}$$

The equation for the velocity of the droplets are therefore characterised by a deterministic and a stochastic part. In the deterministic part $\mathbf{V}^{(i)}$ is the velocity vector of the $i-th$ particle, $\widetilde{\mathbf{U}}$ the resolved gas phase velocity, ρ_g, ρ_l the densities of gas and liquid phase respectively and $\mathbf{g}$ is the gravitational acceleration vector. The relaxation time for the particle is defined as $\tau_p^{-1} = \frac{3}{8}C_D\frac{\rho_g}{\rho_\ell}\frac{|\widetilde{\mathbf{U}}-\mathbf{V}^{(i)}|}{r_p^{(i)}}$ where the drag coefficient is obtained from Yuen-Chen [19], and r_p is the radius of the particle. The stochastic part is represented by the increment of a Wiener process $d\mathbf{W}_t$, C_0 is a model constant, assigned a value of unity, k_{sgs} is the modelled unresolved kinetic energy of the gas phase, and τ_t is the sub-grid time scale, which modulate the dispersion rate introduced by the Wiener process, defined as:

$$\tau_t = \frac{\tau_p^{1.6}}{\left(\Delta/\sqrt{k_{sgs}}\right)^{0.6}} \tag{6}$$

The approach has been applied extensively and successfully in previous work, eg [20, 21]. The droplet evaporation is simulated using an equilibrium model [22, 23]. In cases where the evaporation rates are low and thus the evaporation is dominated by mass transfer effects, a homogeneous internal temperature distribution may be assumed in the droplet and phase equilibrium conditions at the surface. Under these assumptions the temperature $\Theta^{(i)}$ and mass $m^{(i)}$ of a single droplet i can be expressed as [24]:

$$d\Theta^{(i)} = \frac{Nu^*}{3Pr_g}\frac{C_{p_g}}{C_{p_\ell}}\left(\frac{\Theta_g - \Theta^{(i)}}{\tau_p}\right)\frac{\ln(1+B_T)}{B_T}dt + \\ + \frac{h_v}{C_\ell}\frac{\dot{m}^{(i)}}{m^{(i)}}dt \tag{7}$$

$$dm^{(i)} = -\frac{Sh^*}{3Sc_g}\left(\frac{m^{(i)}}{\tau_p}\right)\ln(1+B_M)dt \tag{8}$$

where C_{p_ℓ} and C_{p_g} are the specific heat capacity of liquid and gas respectively, h_v is the latent heat of evaporation, B_T and B_M are respectively the heat and mass transfer Spalding numbers. The classic rapid mixing evaporation model with Stefan flow included is adopted. The liquid properties are evaluated using the $1/3^{rd}$ rule. Nusselt (Nu^*) and Sherwood (Sh^*) numbers are modified such that they are the sum of a deterministic plus a stochastic term, this to include the effects of the unresolved fluctuations on mass and temperature evolution. The deterministic term is obtained by the Ranz-Marshall correlation [25], while the stochastic contribution is:

$$Sh^{st}dt = Nu^{st}dt = \sigma_g^{1/3}\left(\rho_g\frac{k_{sgs}^{1/2}D}{\mu_g}\right)|dW_t|^{1/2}\tau_p^{3/4} \tag{9}$$

where σ_g is the gas phase Schmidt or Prandtl number as appropriate.

3. Experimental and Numerical Configuration

3.1. Experimental Configuration

The experimental configuration which is described in detail in [8, 9], comprises a cylindrical hot co-flow generator which burns Dutch Natural Gas (DNG) to increase the airflow temperature. Different cases are provided depending on the boundary conditions in terms of fuel flow rate, co-flow temperature and velocity. However, the results in all cases are similar and the focus of this work is thus on a single case. Details of the fuel and co-flow of the different simulated cases are summarised in Table 1, for further information the reader is referred to [8, 9]. In the centre of the co-flow generator a commercial hollow cone injector is located as it is shown in the non scaled schematic, Fig. 1.

Case	$T_0[K]$	$U_{cf}[m/s]$	$O_2[\%]$	$\dot{m}[kg/s]$
H_I	1,480	3.42	7.1	3.7 E-4
H_{II}	1,300	2.23	9.3	4.0 E-4
H_{III}	1,225	1.81	10.1	4.1 E-4

Table 1: Details of different simulated cases: co-flow temperature, co-flow axial velocity, co-flow oxygen percentage in mass, and injected fuel flow rate. [8, 9].

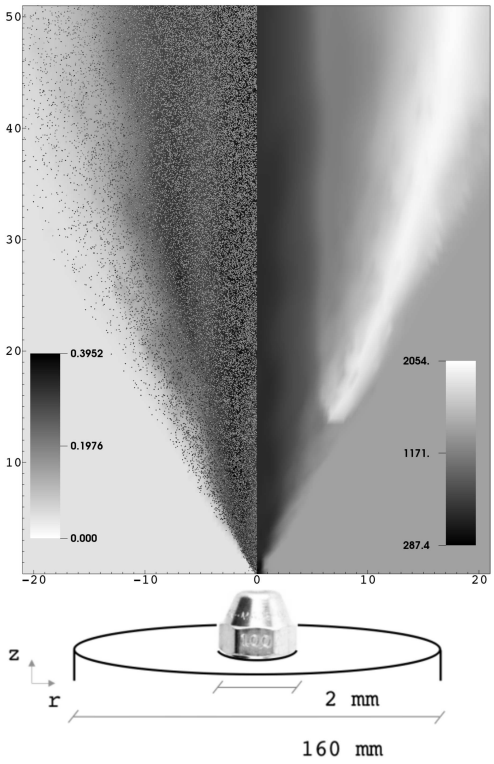

Figure 1: Non scaled schematic of the injector at the bottom, pseudo-colour profile of temperature (right) and mixture fraction (left) obtained from simulations. Dots on the left-half represent droplets.

3.2. Numerical Details

The simulations were performed using Boffin-LES in-house code; the computational domain is a cylinder with dimensions ($3D \times 10h$) where D is the diameter ($80mm$) of the experimental configuration and h ($50mm$) is the height of the furthermost downstream measurement location. The mesh consists of 180 blocks and $\sim 3.50 \cdot 10^6$ elements, in the horizontal plane the mesh is arranged to be finer near the injector (with $\sim 0.34mm$ spacing) and coarser towards the edges (with $\sim 1.5mm$ spacing). In the axial direction the grid is uniform, with a spacing $\sim 0.4mm$, in the region extending to the furthermost downstream measurement location and then expands downstream with an exponential growth maintaining low aspect ratio ($< 8\%$) such that the commutation errors are negligible. Inlet boundary conditions are provided by

the experimental database for the continuous phase and free slip conditions are applied at the outer sides of the domain. A synthetic turbulence generator, [10] is used, based on the measured profiles at the inlet. The droplets injected from the nozzle are characterised by an inhomogeneous distribution in terms of diameter, injection angle, and velocities. A description of the injector based on the experimental information available at the first measurement location was developed in this work. The proposed model aims to represent the inhomogeneous behaviour of small droplets ($d < d_h = 30\mu m$) where d_h is the observed threshold for homogeneous behaviour. The droplet size distribution is based on a random variable $d^{(i)} = x_1$ which is sampled from a Rosin-Rammler distribution $x_1 \sim f\left(d; \chi, q\right)$ with χ being the Sauter Mean Diameter (SMD) ($\chi = 45\mu m$) and q a dispersion factor ($q = 3$). The injection angle, $\psi(d)$ is conditioned on the diameter and depends on the nominal injection angle ($\mu = 30°$) and the standard deviation ($\sigma = 15°$):

$$\begin{aligned} \psi(d) &= \mu + \sigma \cdot x_2 \\ x_2 &= f\left(\omega; 0, 1\right) * G\left(\omega\right) \\ G\left(\omega\right) &= H\left(\omega - \sigma^{-}\right) - H\left(\omega - 1\right) \\ \sigma^{-} &= \begin{cases} \frac{d}{d_h} - 2 & \text{if } d < d_h \\ -1 & \text{if } d > d_h \end{cases} \end{aligned} \tag{10}$$

where the random variable x_2 is sampled from a distribution $\mathcal{N}^*\left(0, 1\right)$ obtained by convolution of the standard normal distribution $f\left(\omega; 0, 1\right)$ with the function $G(\omega)$; where H is the Heaviside function and ω is the random variable.The correction collapses to a standard normal distribution when the diameter reaches d_h and the jet then assumes homogeneous features. A graphical representation of this model is presented in Fig. 2. The same principle is applied for the injection velocity via a piecewise continuous function defined as:

$$\left|\mathbf{V}^{(i)}\right|\left(d\right) = \begin{cases} \frac{v_M - v_m}{d_h} d + v_m & \text{if } d < d_h \\ v_M & \text{if } d > d_h \end{cases} \tag{11}$$

where the minimum, v_m and maximum, v_M velocities are measured quantities. The practice of assuming a droplet distribution defined in terms of the SMD and dispersion factor obtained from empirical correlations is clearly limited. However, the conditional injection model is based only on the parameter d_h and results are relatively insensitive to its value.

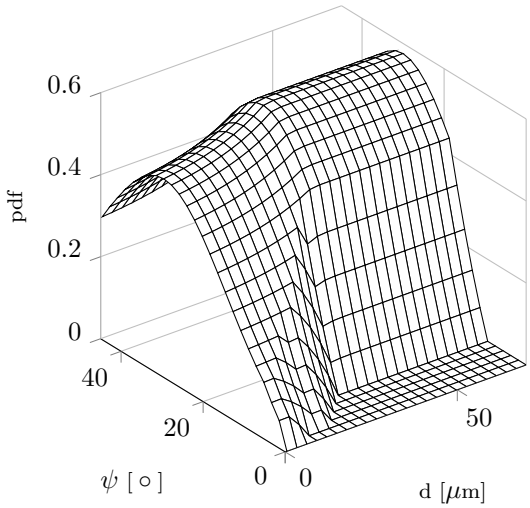

Figure 2: Injection pdf of droplets correlating diameters with injection angle.

4. Results

Results were obtained with constant time step of $(1 \cdot 10^{-7} s)$ resulting in a maximum Courant number of 0.17. The flow was allowed to develop for 15 flow through times without the spray, (based on the bulk velocity $2.5 m/s$ and h) and 10 additional flow through times with spray were computed. Data statistics were collected over 10 flow through times and averaged circumferentially. Simulations were performed using 180 cores on a Cray XC30 Supercomputer providing 100 time steps per hour.

4.1. Continuous Phase

Radial temperature profiles of H_I and H_{III} cases at different axial locations are presented in Fig. 3, while the H_{II} case is presented in Fig. 4. The co-flow temperature (T_0) and the LOH for the different cases are summarised in Table 2. The temperature profiles, both simulated and measured, are qualitatively

Case	Exp LOH [mm]	LES LOH [mm]
H_I	8	9
H_{II}	13	13
H_{III}	18	17

Table 2: Co-Flow temperature and Lift-off for different test cases.

very similar in all three cases. The simulations show a slight outward shift in the location of the maximum temperatures and an under estimation of the temperature along the centreline compared with the measurements. However, the onset of the flame is accurately reproduced in all cases and the maximum temperatures and their locations are in excellent agreement with the measurements up to $z = 20mm$. Beyond this location

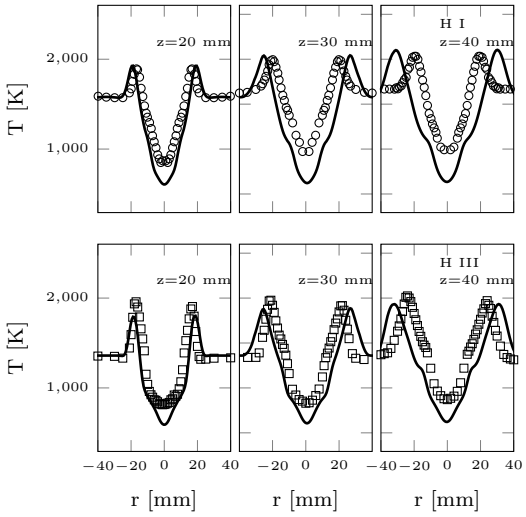

Figure 3: Comparison of radial temperature profiles at different axial locations for simulated H_I ($\circ$) and H_{III} ($\square$) cases with the measurements ($-$).

it is possible to observe a radial displacement of the peak that results in an over prediction of the spreading rate of the flame. In the vicinity of the centreline a local minimum is observed which is due to the absorption of heat from the spray phase. The flame exhibits an outer and inner flame front separated by a flame of $\sim 4[mm]$. The simulated flames are all in excellent agreement with measurements in terms of LOH, Table 2. Case H_{II} has a lift-off height of $13mm$, which is in almost perfect agreement with the experimental measurements. This parameter has been calculated considering the mean temperature profile and computing the distance between the injector tip and the first temperature maximum. As the results are very similar for all three cases as observed in the temperature profiles, in the remainder of the paper only results for case H_{II} will be presented. Instantaneous snapshots of temperature and mixture fraction for this flame are shown in Fig. 1. The Root Mean Squared (RMS) temperature fluctuation are presented in Fig. 5 and show that a maximum in the fluctuations occurs in the region close to where the flame originates. The intensity of the fluctuations decays with downstream distance, as the flame stabilises further downstream. The simulations exhibit excellent agreement with measurements. The spray, injected at ambient temperature ($T_{inj} = 301K$) evaporates lowering the continuous phase temperature. Once the gas phase surrounding the droplets becomes increasingly rich in fuel vapour, the evaporation rate decreases and therefore the droplets can travel further downstream before completely evaporating. In the left side of Fig. 1 it is possible to observe the mixture fraction distribution in a plane containing the centreline. Small droplets are "trapped" in the flame while bigger droplets (white) escapes, the small droplets move in the axial direction and result in the mixture fraction reaching saturation levels. If the local mixture fraction falls below this value, then

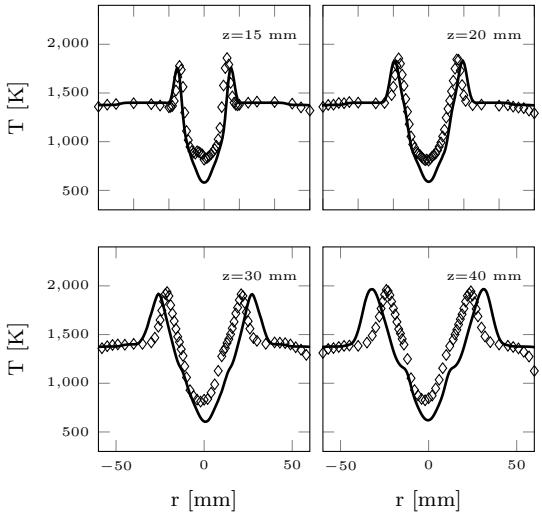

Figure 4: Radial profile of temperature of H_{II} at different axial locations, ($\diamondsuit$) for the measurements, ($-$) for the simulation.

the droplets will evaporate very rapidly due to their small mass and high temperature. In [8, 9] droplets with diameter $d < 6\mu m$ are used as tracer for the gas phase velocity as the Stokes number is below unity. This technique was mimicked in the simulation with droplet statistics being obtained over five flow through times. The results obtained were, as expected, almost identical to the values obtained by averaging the computed gas phase velocity. However, in regions where no droplets are present it is not possible to obtain information about the gas phase velocity by the tracking of small droplets. The results from the gas phase simulation are thus used for comparison with the measured profiles shown in Fig. 6, where good agreement is evident.

4.2. Dispersed Phase

Comparison between experimental and simulated radial profiles of axial and radial velocities per different class sizes are presented in Fig. 7 and Fig. 8 respectively. The spray comprises a jet with a structure that is reflected in the profiles of droplet axial velocity. The maximum velocity indicates an angle of spread of $\sim 25°$, with droplets evaporating as they travel downstream thus losing momentum and dispersing towards the side of the flame into a low gas velocity zone. The simulated droplet axial velocities for the $10\mu m$ and $20\mu m$ classes are somewhat too large compared with the measurements beyond $z = 20mm$ from the injector tip. The profiles suggest that only small droplets are entrained in to the centreline region of the flame while bigger ones have a "ballistic" trajectory. Figure 9 presents the radial profiles of the droplet size SMD at different axial locations. The agreement between measured and simulated profiles of SMD is generally good with the measurements suggesting that the simulated SMD may be too low in the immediate vicinity of the

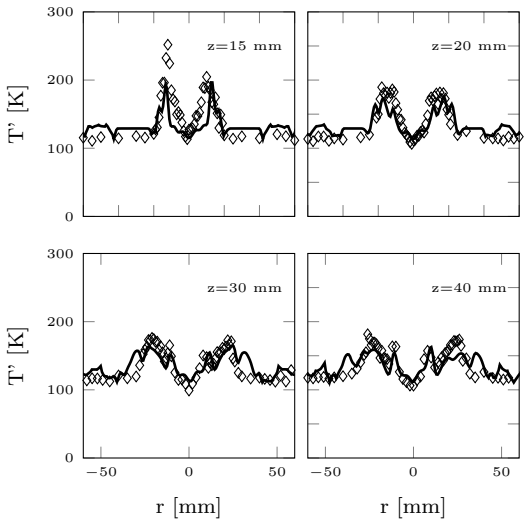

Figure 5: Radial profile of temperature RMS at different axial locations, (♢) for the measurements, (−) for the simulation.

centreline, possibly caused by an over estimation of the evaporation rates.

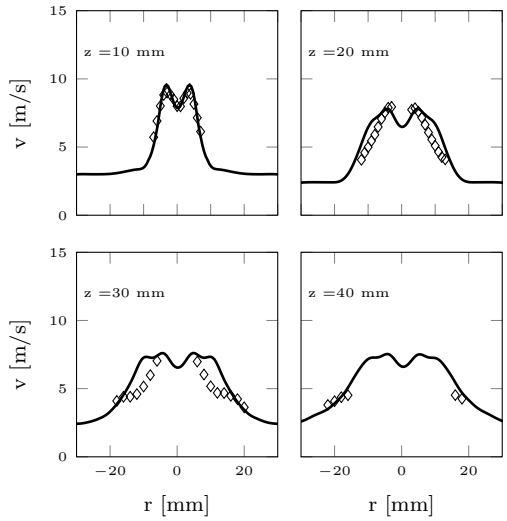

Figure 6: Radial profile of the gas phase velocity at different axial locations. ($\diamondsuit$) for the measurements, ($-$) for the simulation.

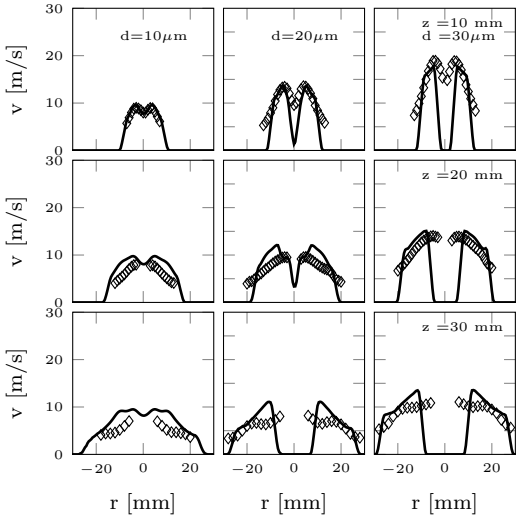

Figure 7: Radial profiles of axial velocities of droplets for different class sizes (columns: $[0\mu m - 10\mu m]$, $[10\mu m - 20\mu m]$, $[20\mu m - 30\mu m]$) and axial locations (rows). ($\diamondsuit$) for the measurements, ($-$) for the simulation.

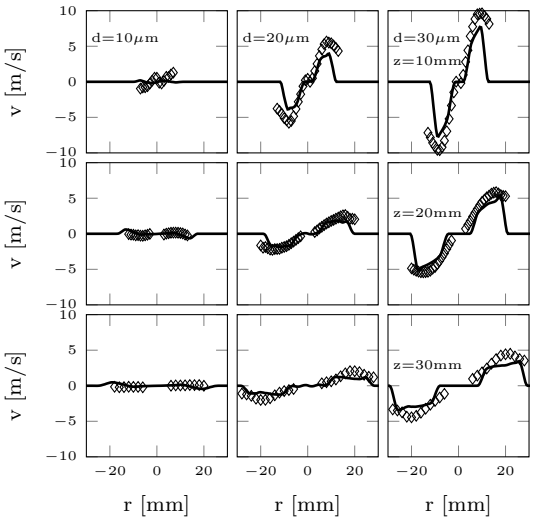

Figure 8: Radial profiles of radial velocities of droplets for different class sizes (columns: $[0\mu m - 10\mu m]$, $[10\mu m - 20\mu m]$, $[20\mu m - 30\mu m]$) and axial locations (rows). ($\diamondsuit$) for the measurements, ($-$) for the simulation.

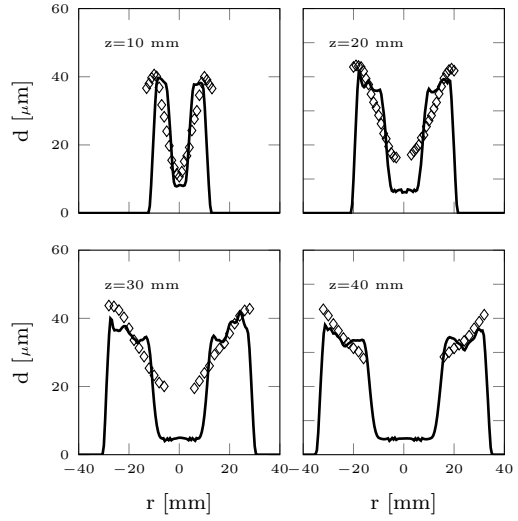

Figure 9: Radial profile of SMD at different axial locations. ($\diamondsuit$) for the measurements, ($-$) for the simulation.

It is observed how values of the SMD increase with increasing downstream distance because of the preferential disappearance of small droplets through evaporation. The maxima in SMD near the outer edges of the flame suggest that only droplets with high mass are present in this region.

5. Conclusion

The simulation of MILD combustion system has been performed in the context of LES-pdf with stochastic field approach together with Lagrangian particles description of the dispersed phase. A comparison of the simulated results with measurements shows overall good agreement. The dispersed phase velocities and SMD are generally well represented by the simulations as is the gas phase velocity. The location of the base of the flames is correctly reproduced for all three cases considered, however a small shift in the maximum temperature is observed beyond $20mm$ from the injector tip. The lack of modelling of the primary break-up is presumed to be a substantial contribution to the observed discrepancies. The injector has been characterised *a posteriori* using the measured properties at the measurement location closest to the injector. The resulting boundary condition applied at the injector were conditioned to the droplet diameter.

6. Acknowledgments

The authors are grateful to General Electrics Power (Switzerland) for their financial support. This work used the ARCHER UK National Supercomputing Service (http://www.archer.ac.uk).

References

[1] A. Cavaliere, M. de Joannon, Prog. Energ. Combust. 30 (4) (2004) 329-366.
[2] J. Wünning, J. Wünning, Prog. Energ. Combust. 23 (1) (1997) 81-94.
[3] M. Katsuki, T. Hasegawa, Proc. Combust. Inst. 27 (1998) 3135-3146.
[4] J. van Oijen, Proc. Combust. Inst. 34 (2013) 1163-1171.
[5] Y. Minamoto, N. Swaminathan, Combust. Flame 161 (4) (2014) 1063-1075.
[6] P. Coelho, N. Peters, Combust. Flame 124 (3) (2001) 503-518.
[7] M. Ihme, Y. C. See, Proc. Combust. Inst. 33 (2011) 1309-1317.
[8] H. Correia Rodrigues, M. J. Tummers, E. H. van Veen, D. J. Roekaerts, Combust. Flame 162 (3) (2015) 759-773.
[9] H. Correia Rodrigues, M. Tummers, E. van Veen, D. Roekaerts, Int. J. Heat Fluid Fl. 51 (2015) 309-323.
[10] M. Klein, A. Sadiki, J Janicka, J. Comput. Phys. 186 (2003) 652-655.
[11] L. Ma, B. Naud, D. Roekaerts, Flow Turbul. Combust. (2015) 1-34.
[12] W. P. Jones, A. Marquis, K. Vogiatzaki, Combust. Flame 161 (1) (2014) 222-239.
[13] W. P. Jones, A. Marquis, D. Noh, Proc. Combust. Inst. 35 (2015) 1685-1691.

[14] S. Gallot Lavallée, W. P. Jones, Flow Turbul. Combust. 96 (2) (2016) 513-534.

[15] U. Piomelli, J. Liu, Phys. Fluids 7 (4) (1995) 893-848.

[16] L. Valiño, Flow Turbul. Combust. (1998) 157-172.

[17] W. P. Jones, S. Navarro-Martinez, Combust. Flame 150 (3) (2007) 170-187.

[18] A. Bhagatwala, J. Chen, T. Lu, Combust. Flame 161 (7) (2014) 1826-1841.

[19] M. C. Yuen, L. W. Chen, Comb. Sci. & Tech. 14 (1976) 147-154.

[20] W. P. Jones, C. Lettieri, Phys. Fluids 22 (11) (2010) 115106.

[21] M. Bini, W. P. Jones, J. Fluid Mech. 614 (2008) 207-252.

[22] W. Sirignano, Prog. Energ. Combust. 9 (4) (1983) 291-322.

[23] G. Faeth, Prog. Energ. Combust. 9 (1) (1983) 1-76 .

[24] R. S.Miller, K. Hastard, J. Bellan, Int. J. Multiphas. Flow 24 (6) (1998) 1025-1055 .

[25] W. Ranz, W. Marshall, Chem. Eng. Prog. 48 (3) (1952) 141-146.